Electrochemical Control of Lithium-Ion Batteries

KANDLER A. SMITH

Batteries help advance technologies ranging from portable electronics to renewable power systems and environmentally friendly vehicles. One such technology is the hybrid electric vehicle (HEV), which uses a battery and an electric motor in conjunction with a combustion engine to increase fuel efficiency. For HEV applications, nickel metal hydride (Ni-MH) battery chemistry is presently the norm. But lithium-ion (Li-ion) chemistry, with roughly twice the power and energy density of Ni-MH, is expected to facilitate new vehicle designs. These designs include plug-in hybrid electric vehicles with a 10–40-mi all-electric range for normal commuting as well as pure battery-powered electric vehicles with up to a 300-mi range and the possibility of fast recharge.

Batteries are often heavy and almost always expensive. Therefore, advances that can overcome these limitations are actively sought from both traditional and nontraditional research disciplines. For control theoreticians and engineers, onboard assessment of battery state of health (SOH), state of power (SOP), and state of charge (SOC) remain open areas of research. Compared to traditional empirical methods, electrochemical model-based methods may improve the accuracy of onboard state estimates, albeit at the cost of additional complexity. But this added complexity may be acceptable if a new algorithm can improve the available power and energy, enabling the battery to be smaller, lighter, and less expensive. For these reasons, Li-ion battery estimation and control is a critical research topic for advancing low-cost, low-carbon technologies.

In practice, batteries must be monitored and controlled based on quantities that can be measured onboard. These measurements are presently limited to current, voltage, and temperature, and thus onboard controllers must estimate internal battery states, such as SOC and SOP, using only these three measurements. This estimation can be based on a battery reference model, which describes current, voltage, and temperature dynamics as a function of the battery's internal states.

To avoid dealing with complex electrochemistry, battery-estimation algorithms typically use a grey-box, empirical reference model to mimic voltage/current dynamics and their dependence on internal states [1], [2]. This battery reference model is in the form of an equivalent circuit, which is easy to identify and tends to agree well with test data under near-equilibrium conditions. SOC, which is related to the lumped chemical resources of the battery at equilibrium, is reasonably predicted by empirical-based estimation algorithms for Li-ion chemistry. But sustained power events, particularly high-power ones, pull the battery far from equilibrium, in which case equivalent circuit models have difficulty matching the battery's behavior.

Traditionally, battery control constraints are defined as do-not-exceed current, voltage, and temperature values, since those quantities are directly measurable. Without knowledge of internal battery physics, embedded controllers manage battery discharging and charging within fixed minimum and maximum voltage limits. But in high-power applications, where discharging and charging are highly transient, these global limits can be unnecessarily conservative.

Estimation and control based on a physically justified electrochemical model can potentially provide more accurate state estimates when the battery is driven far from equilibrium. This improved accuracy relative to equivalent circuit methods may help detect internal faults without adding extra sensors or circuitry. In addition, electrochemical state estimation can provide a means for managing the battery within its true limits of operation and thereby expand its performance. A supervisory controller observing an electrochemical constraint might, for example, allow discharge up to a lithium depletion limit at the electrochemical reaction interface, which can enable greater discharge power compared to a fixed minimum-voltage constraint. Since the localized lithium concentration is internal to the battery, it cannot be measured directly but instead must be estimated by means of an electrochemical reference model.

Electrochemical models reasonably predict Li-ion battery performance and physical limits across a wide range of operating conditions [3]. The main difficulty for their onboard application is solving the coupled nonlinear partial differential equations (PDEs) of the model in a timely fashion. The model-based state algorithm needs to take into account diffusion dynamics, which govern voltage/current behavior, across a range of time scales from tens of minutes down to a tenth of a second. We thus describe an approach for electrochemical model reduction [4], [5], estimation, and control of Li-ion batteries [6]. We begin with a brief description of Li-ion battery physics.

Digital Object Identifier 10.1109/MCS.2010.935882

1066-033X/10/$26.00©2010IEEE

LI-ION PHYSICS

Figure 1 shows a cutaway of a Li-ion battery, which is called a cell in the electrochemical literature. To construct the cell, a slurry of negative electrode active material, typically graphite, is coated onto a copper foil. Another slurry of positive electrode active material, typically a metal oxide, is coated onto an aluminum foil. A doctor blade scrapes the electrodes to a desired thickness. A web-handling machine inserts a polymer separator between the two electrodes and winds the resulting sandwich into a spiral jelly roll. Alternative manufacturing processes [7] fold or stack the electrodes to achieve a prismatic shape.

The wound jelly roll is inserted into a can, and the electrode foils are ultrasonically welded or otherwise connected to the cell's positive and negative terminals. The can is filled with a liquid electrolyte, which seeps into and occupies the pores within the electrodes and separator. Some cells employ a gel electrolyte, which is impregnated into the electrodes and separator before cell assembly. These lithium polymer cells operate on the same principles as their liquid electrolyte Li-ion counterparts.

While electrode materials and specific electrolyte recipes may vary, the basic working principles of all Li-ion batteries are the same. During discharge (the bottom of Figure 1), solid-phase Li diffuses to the surface of the negative electrode active material, where it undergoes an electrochemical reaction that transfers Li^+ ions into the electrolyte solution. In the case of graphite, this reaction is

$$Li_xC_6 \underset{\text{charge}}{\overset{\text{discharge}}{\rightleftharpoons}} Li_0C_6 + xLi^+ + xe^-.$$

The Li^+ ions travel through the electrolyte phase by diffusion and ionic conduction to the positive electrode, where they again react and transfer back to the solid phase. The reaction at the positive electrode is

$$Li_0MO_2 + yLi^+ + ye^- \underset{\text{charge}}{\overset{\text{discharge}}{\rightleftharpoons}} Li_yMO_2,$$

where MO_2 is a metal oxide. The solid-phase Li then diffuses from the surface of the metal oxide particles to the interior. The porous separator, which serves as an electronic insulator between the positive and negative electrodes, forces electrons to follow an opposite path to the Li^+ ions, which is through an external load. The composite electrodes (not shown in Figure 1) usually contain inert additives to enhance electron transport across each porous electrode matrix and to accommodate shrinking and swelling of the materials during cycling.

During sustained discharge of the battery, lithium concentration gradients build across the cell as shown in Figure 1. This concentration-gradient-induced polarization lowers the working voltage of the cell beneath its equilibrium voltage, which also reduces its energy efficiency. During high-current discharge, the cell can suddenly lose power output if the concentration of lithium is either saturated or depleted

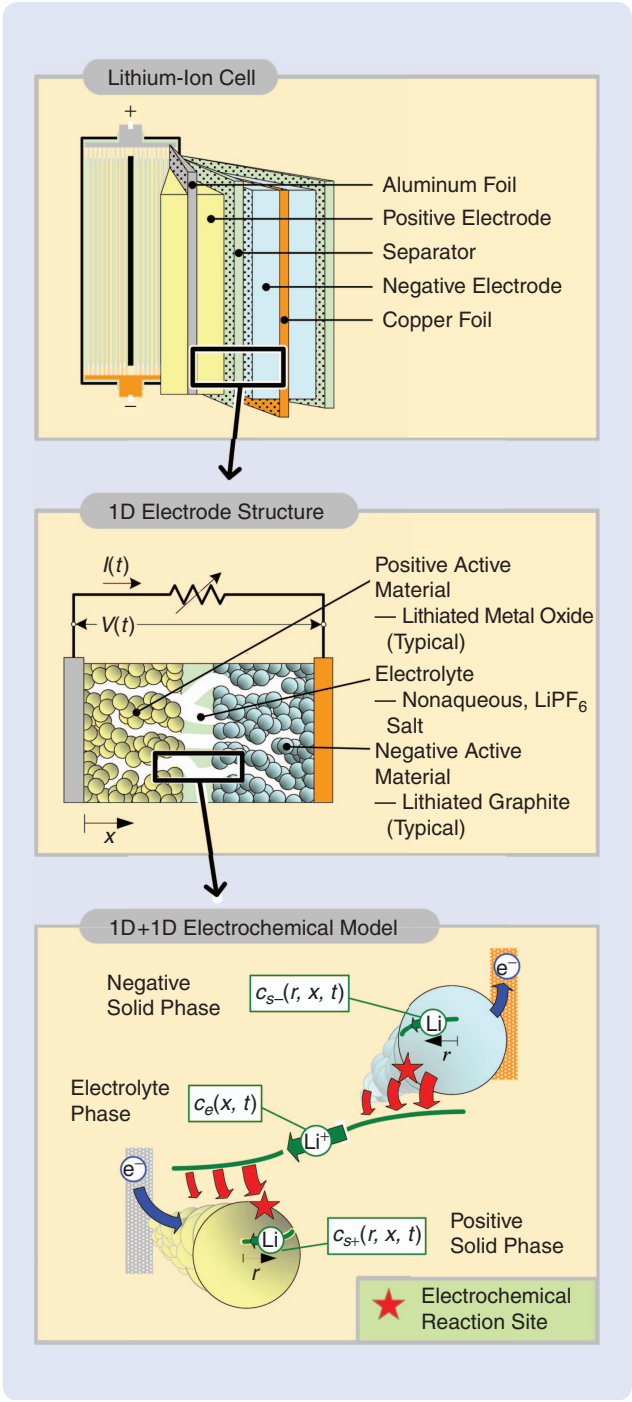

FIGURE 1 Internal structure and operation of a Li-ion cell. Electrons travel to and from cell-interior regions by means of copper and aluminum foils. During the electrochemical discharge process (bottom window), Li diffuses to the surface of negative-electrode particles and undergoes an electrochemical reaction. This reaction releases an electron and transfers Li to the electrolyte phase. The Li^+ ions diffuse and conduct through the electrolyte solution to the positive electrode, where a similar reaction transfers Li to the positive solid phase. Li is stored inside the positive electrode particles until the cell is later recharged. The 1D+1D electrochemical model describes reaction kinetics for the transfer of Li between phases and concentration gradients, that is, transport of Li within each phase.

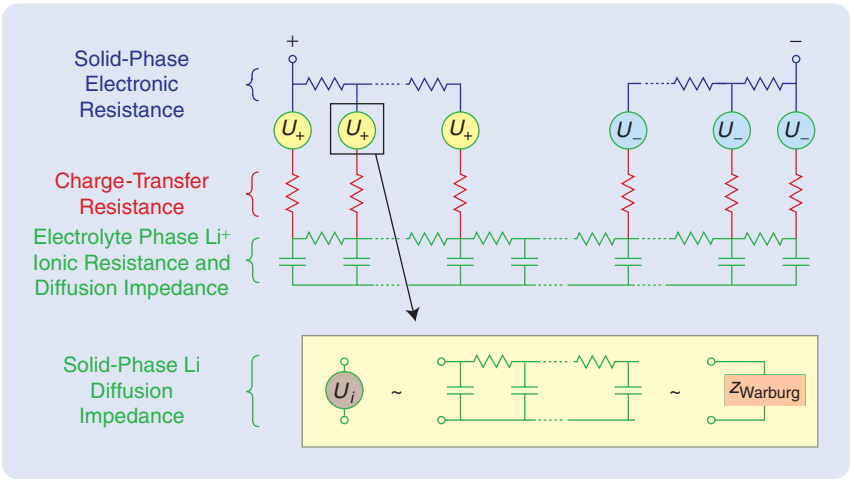

FIGURE 2 Approximate circuit showing factors that contribute to the small-signal impedance of a Li-ion cell. Capacitors represent Li accumulation in localized regions of the solid and electrolyte phases. The inset shows solid-phase diffusion modeled using a Warburg fractional circuit element, which has the constant-phase property [8].

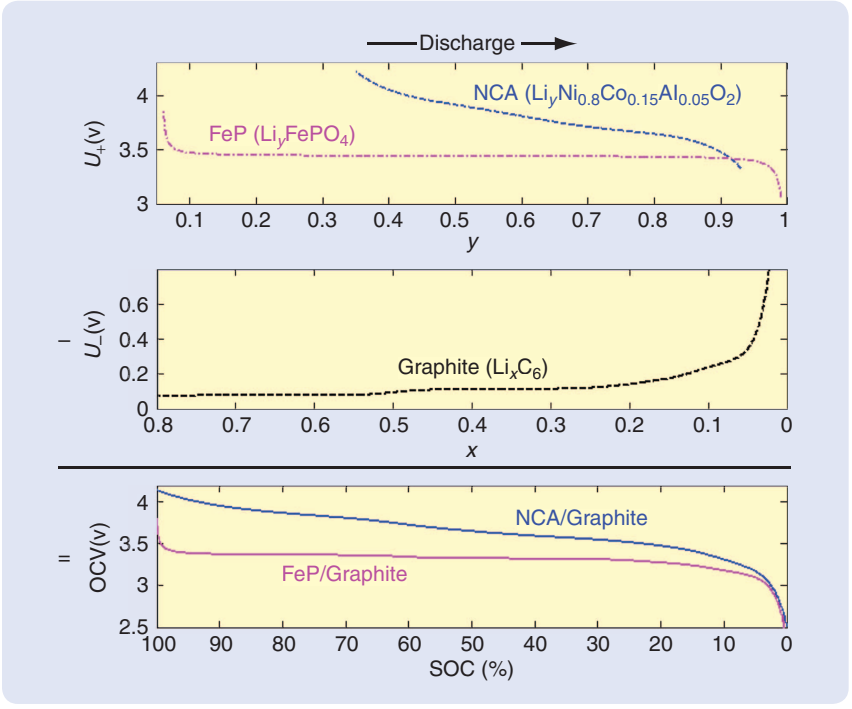

FIGURE 3 Li-ion cell open-circuit voltage (OCV). The OCV is determined by the positive electrode equilibrium potential U_+ minus the negative electrode equilibrium potential U_-. Electrode stoichiometries x and y are linearly related to the state of charge (SOC) and vary within the ranges shown. The OCV depends on the electrodes' surface SOC, which is equal to the cell's average SOC only at equilibrium.

at the electrode/electrolyte interface. These transport limitations make the cell appear to have run out of energy even though substantial energy might remain at a lesser discharge rate or following a period of rest.

VOLTAGE/CURRENT DYNAMICS

Cell design, including choice of materials and geometry, contributes to the cell's small-signal impedance, that is, the voltage response measured for a small current perturbation at the cell terminals. Geometric factors dictating cell impedance include electrode thickness, active material particle size, and electrolyte pore size. This impedance changes with time, governed by diffusion processes taking place inside the cell. It is also distributed, analogous to a long transmission line with a wide range of time constants. Alternating current impedance can be characterized using electrochemical impedance spectroscopy (EIS) methods [8].

Figure 2 provides a circuit analogy for the cell, showing the various contributions to impedance, such as solid-phase electron and Li transport, charge-transfer reaction kinetics, and electrolyte-phase Li^+ transport. In reality, the resistor and voltage source elements in Figure 2 depend nonlinearly on Li concentration, with those concentration dynamics governed by diffusion processes. For real-time application, the circuit shown in Figure 2 is often reduced to just one resistor and capacitor pair, which approximates the dynamics of three separate diffusion processes, and one voltage source, which approximates the equilibrium potential of two separate electrodes.

At equilibrium, the cell's voltage depends on the total amount of charge stored in the cell, that is, the average Li concentration of the two electrodes. A lumped charge-conservation analysis shows that, neglecting slow side reactions, the two electrodes' average concentrations are always linearly related to one another. Following discharge/charge at room temperature, it may take tens of minutes for all Li and Li^+ concentration gradients to relax and establish equilibrium. At cold temperatures, equilibrium may take several hours due to sluggish solid-phase diffusion.

At full equilibrium, the cell's open-circuit voltage (OCV) can be measured and used to infer SOC. The active materials chosen for the two electrodes dictate the OCV of the cell and how it changes with SOC. The OCV of the cell is equal to the difference between the positive and negative electrodes' equilibrium potentials. Figure 3 shows the equilibrium potential U of graphite and two common positive electrode materials, nickel-cobalt-aluminum oxide (NCA)

and iron-phosphate (FeP). Potentials are measured relative to pure metallic-phase Li. Equilibrium potential varies with active material stoichiometry, that is, the degree to which each material is filled with Li. At high SOC, the negative electrode's host sites are nearly full, that is, *intercalated*, with Li, while the positive electrode sites are nearly empty, that is, *de-intercalated*, and thus ready to accept and store Li as it transfers across from the negative electrode during discharge.

With a known OCV/SOC relationship, a voltage measurement can be used to estimate SOC, although this relationship is valid only when the cell is at full equilibrium. While the cell is being cycled, this initial voltage-based SOC estimate can be carried forward in time by integrating the current entering and leaving the cell. To avoid error accumulation due to sensor-measurement error, model-based state algorithms can be used to refine the state estimate during dynamic operation using current and voltage measurements.

It is important to note that electrode equilibrium potentials vary as functions of electrode surface SOC, not average SOC. Equivalent circuit models that schedule their RC parameters as a function of average SOC do not properly capture nonlinearities when far from equilibrium. Compared to average SOC, surface SOC is a more dynamically varying quantity and is actually more observable, as indicated by the observability/controllability gramian of a balanced realization model [6]. Since surface SOC is physically related to the instantaneous power capability of the cell, it is desirable to estimate and use this quantity as an electrochemical control constraint.

Batteries with a flat OCV/SOC relationship, such as those using FeP chemistry as shown in Figure 3, present a significant challenge for online estimation. This particular chemistry is also known to exhibit voltage hysteresis in its OCV/SOC relationship. State estimation is most difficult for the FeP chemistry in HEV-type applications, where the battery is operated within a 30–70% SOC window, the flattest region of Figure 3. But strong discharge or charge events regularly pull the electrode surface SOC outside this flat area. Thus the need arises to refine state estimates by means of a model that provides sufficient accuracy at states far from equilibrium.

ELECTROCHEMICAL MODEL REDUCTION

Identification of a low-order electrochemical model is necessary for embedded model-based control. Control systems for automotive applications, for example, require an update rate of around 10 Hz. An explicit rather than iterative solution of the electrochemical reference model is thus desirable.

The four-PDE electrochemical battery model [3] describes conservation of lithium in the solid phase

$$\frac{\partial c_s}{\partial t} = \frac{D_s}{r^2}\frac{\partial}{\partial r}\left(r^2\frac{\partial c_s}{\partial r}\right), \tag{1}$$

conservation of lithium in the electrolyte phase

$$\frac{\partial(\varepsilon_e c_e)}{\partial t} = \frac{\partial}{\partial x}\left(D_e\frac{\partial}{\partial x}c_e\right) + \frac{1-t_+^o}{F}j^{Li}, \tag{2}$$

conservation of charge in the solid phase

$$\frac{\partial}{\partial x}\left(\sigma\frac{\partial}{\partial x}\phi_s\right) - j^{Li} = 0, \tag{3}$$

and conservation of charge in the electrolyte phase

$$\frac{\partial}{\partial x}\left(\kappa\frac{\partial}{\partial x}\phi_e\right) + \frac{\partial}{\partial x}\left(\kappa_D\frac{\partial \ln c_e}{\partial x}\right) + j^{Li} = 0. \tag{4}$$

These PDEs provide temporal and spatial descriptions of solid and electrolyte-phase lithium concentrations $c_s(r,x,t)$ and $c_e(x,t)$ as well as potentials $\phi_s(x,t)$ and $\phi_e(x,t)$. Parameters appearing in (1)–(4) are diffusion coefficients of Li/Li^+ in the solid/electrolyte phases, respectively, D_s and D_e, electrolyte volume fraction ε_e, electrode electronic conductivity σ, electrolyte ionic conductivity κ, and electrolyte diffusional conductivity κ_D. The Butler-Volmer equation

$$j^{Li} = a_s i_o\left\{\exp\left[\frac{\alpha_a F}{RT}\eta\right] - \exp\left[-\frac{\alpha_c F}{RT}\eta\right]\right\} \tag{5}$$

relates reaction rate j^{Li} as a function of overpotential η defined by

$$\eta = \phi_s - \phi_e - U. \tag{6}$$

Overpotential is the driving force for an electrochemical reaction. In (5), a_s is the solid/electrolyte interfacial area per unit volume, F is the Faraday constant, R is the universal gas constant, and T is absolute temperature. A double-layer capacitance effect is occasionally included in (3) and (4), although that effect can usually be neglected at times longer than a millisecond [9].

For practical use, the order of (1)–(4) must be reduced. Most commonly, spatial discretization techniques, such as finite element or finite volume methods, are employed to reduce the infinite-dimensional system (1)–(4) down to a finite number of unknowns for which solution is possible. However, spatial discretization techniques yield an iterative and often large-order model, which is too computationally intensive for real-time applications.

Beginning with the physical governing equations, Figure 4 outlines a procedure for identifying a reduced-order nonlinear state-variable model of a Li-ion cell [4], [5]. Model reduction is performed in the frequency domain, which, compared to time-domain reduction techniques, ensures that the resulting model is independent of the choice of input. The current $\bar{I}(s)$ is used as model input rather than voltage $\bar{V}(s)$. This structure is necessary because the output/input relationship $\bar{V}(s)/\bar{I}(s)$ is strictly proper, whereas $\bar{I}(s)/\bar{V}(s)$ is not.

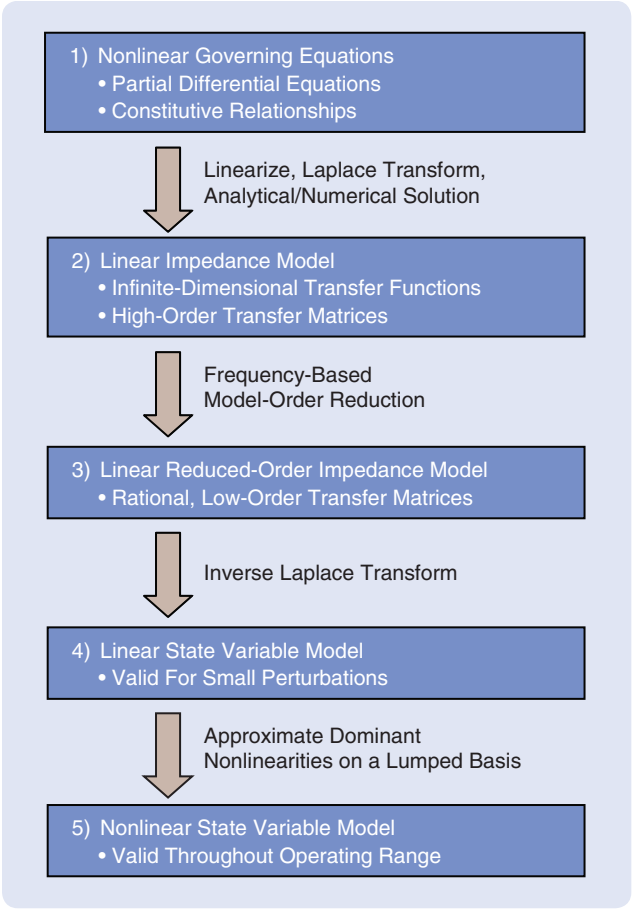

FIGURE 4 Procedure for identifying a reduced-order electrochemical model of a Li-ion cell [4], [5]. Order reduction is accomplished by fitting the infinite-dimensional model's frequency response with a low-order model. Physical knowledge of the system is used to combine local linear models into an approximate global nonlinear model.

Using Laplace transforms, analytical and numerical solutions to the governing equations (1)–(4) yield an infinite-dimensional impedance model in step 2 of Figure 4. This model consists of transfer functions and matrices $\overline{\mathbf{y}}(s)/\overline{I}(s)$ that describe the output response of an electrochemical field variable $\overline{y}(x,s)$ to the input current $\overline{I}(s)$ at discrete locations across the electrode $x = x_i$. In step 3, the high- or infinite-order transfer matrices are reduced to low-order transfer functions of the form

$$\frac{\overline{\mathbf{y}}^*(s)}{\overline{I}(s)} = \mathbf{z} + \sum_{k=1}^{n} \frac{\mathbf{r}_k s}{s - \lambda_k}, \tag{7}$$

where the steady-state vector $\mathbf{z}$ is obtained from the full-order model as $\mathbf{z} = \lim_{s\to 0} \overline{\mathbf{y}}(s)/\overline{u}(s)$ and the eigenvalues λ_k and residue vectors $\mathbf{r}_k$ are numerically generated to minimize the cost function

$$J = \sum_{k=1}^{m} \sum_{i=1}^{n} |\operatorname{Re}(\overline{\mathbf{y}}_i^*(j\omega_k) - \overline{\mathbf{y}}_i(j\omega_k))|^2 + |\operatorname{Im}(\overline{\mathbf{y}}_i^*(j\omega_k) - \overline{\mathbf{y}}_i(j\omega_k))|^2, \tag{8}$$

across the frequency range $\omega \in [0, 2\pi f_c]$. The model's cutoff frequency f_c is chosen to satisfy the bandwidth required by the control application. The Levenberg-Marquart algorithm is used for the minimization [4].

Figure 5 illustrates the model-reduction procedure [5]. The frequency response of the transfer function for negative electrode solid-phase diffusion impedance $\partial U_-/\partial c_s \times \Delta\overline{c}_{s,e-}(x,s)/\overline{I}(s)$ is fit from 0 to 10 Hz. Several additional transfer functions are similarly fit and combined to form a model of the cell's voltage response. This numerical procedure is then repeated at various setpoints to identify local linear models across the range of battery operating conditions. To create a nonlinear voltage/current model (step 5 of Figure 4), parameters of the local linear models are stored in lookup tables and scheduled as functions of positive and negative electrode surface SOC and temperature. It is prudent to check the validity of the nonlinear reduced-order model for cases where spatially varying nonlinearities might be significant. For example, [5] demonstrated model disagreement when electrolyte depletion occurs in either electrode, that is, under sluggish electrolyte transport conditions. Spatial nonlinearities might also be significant at low temperatures, particularly for energy-optimized designs with thick electrodes.

Compared to a higher order finite-volume model, the reduced-order model predicts current/voltage behavior for a 6-Ah HEV cell with less than 2% error [5], including at high discharge and charge rates far from equilibrium. In addition to capturing current/voltage dynamics, the state-variable model provides predictions of concentration and potential field variables within 10%. For the 6-Ah cell, the model order can range from four to seven states depending on the accuracy required. The reduced model runs almost 1000 times faster than a conventional finite-volume model of the same governing equations. The reduced model executes in approximately 1 ms per time step when run in Matlab Simulink on a desktop PC.

At a given temperature, the nonlinear state variable model takes the form

$$\dot{\mathbf{x}} = \lambda \mathbf{x} + I, \tag{9}$$
$$\mathbf{y} = f(\mathbf{x}, I), \tag{10}$$

where $\boldsymbol{\lambda}$ is a diagonal matrix of eigenvalues and the function f interpolates between local linear models. The model output $\mathbf{y}$ can represent cell voltage $V(t)$, an electrochemical field variable, or any combination. If (9), (10) is linearly observable, then (9) can have only one eigenvalue at the origin. This integrator state represents SOC, from which the average concentrations of each electrode can be calculated. All other eigenvalues are real and negative, which is typical of diffusion processes. These stable states represent concentration gradients across the system. Absolute values of concentration, if needed, can be recovered from conservation laws.

For convenience, the model schedules its nonlinearities in the output equation. This simplification is possible because the model reduction is relatively insensitive to the placement of a few numerical eigenvalues that represent tens of thousands of analytical eigenvalues in the model's truncated frequency range of interest. Placing all nonlinearities in the output equation gives the model a fast, explicit solution and streamlines its implementation in an extended Kalman filter estimation algorithm. As shown in [6], and [10], the extended Kalman filter can converge in 10–20 s and produce stable estimates in the presence of current and voltage sensor noise.

ELECTROCHEMICAL CONSTRAINT MANAGEMENT

For estimation and control applications, the model needs to retain only field variables relevant to the control problem of interest. The goal is to utilize the battery up to its true physical limitations and thereby expand usable power and energy.

With respect to electrochemical constraints, the true physical limit of discharge (respectively, charge), accompanied by a sudden voltage decay (respectively, rise), occurs when Li concentrations at an electrodes' surface become saturated or depleted or when the electrolyte Li^+ concentration becomes depleted.

To avoid sudden loss of power, it is thus necessary to avoid depletion or saturation at either electrode surface, which is expressed by

$$0 < \frac{c_{s,e}(x,t)}{c_{s,\max}} < 1. \tag{11}$$

Here, the subscript "s,e" refers to the Li concentration at the solid-electrolyte interface, that is, the electrode surface. It is also necessary to avoid Li^+ depletion in the electrolyte as expressed by

$$c_e(x,t) > 0. \tag{12}$$

In the case of electrode surface depletion/saturation, those conditions are first encountered at the specific value of x where the electrode interfaces with the separator. In contrast, electrolyte depletion first occurs on the opposite side of the electrode, at its interface with the current collector. Once established, the depletion/saturation conditions propagate across the electrode.

To prevent damage to the battery, each electrode's phase potential difference must be maintained within potential limits that define regions where deleterious side reactions do not occur, that is,

$$U_{\substack{\text{side rxn}\\ \text{deinsertion}}} < \phi_s(x,t) - \phi_e(x,t) < U_{\substack{\text{side rxn}\\ \text{insertion}}}. \tag{13}$$

Internal temperature [11] and material stress limitations [12], [13] can also be considered for constraint management.

Depending on the cell's design, only a few of the above limitations may come into play. In the discharge direction, negative surface depletion and positive surface saturation are both common. In the charging direction, it is necessary to avoid side reactions that degrade the cell. In the extreme overcharge case, it is possible to initiate exothermic reactions that generate excessive heat and send the cell into thermal runaway.

For efficient integration into a system, it is convenient for the battery state algorithm to report internal constraints in terms of quantities meaningful to the supervisory controller, for example, the maximum charge or discharge current that can be sustained by the battery. A reference governor [14] can eliminate the need for the supervisory controller to control the battery in terms of electrochemical quantities. The reference governor performs simulations to determine how much charge/discharge is allowed without exceeding a constraint.

The reference governor can report a current that is available within constraints either on an instantaneous basis or one that is available for some seconds into the future. In many situations, a linear reference current governor may be sufficient. Though less precise than a nonlinear governor, the linear calculation requires less computational overhead. For the 6-Ah HEV battery implementation, the complete algorithm, which combines a seventh-order nonlinear state model, an extended Kalman filter, and a linear reference governor, runs in less than 5 ms/timestep in Matlab Simulink on a standard PC.

Manufacturer data sheets typically establish battery-charging rate limits by defining a maximum voltage not-to-be-exceeded during operation. This fixed voltage limit

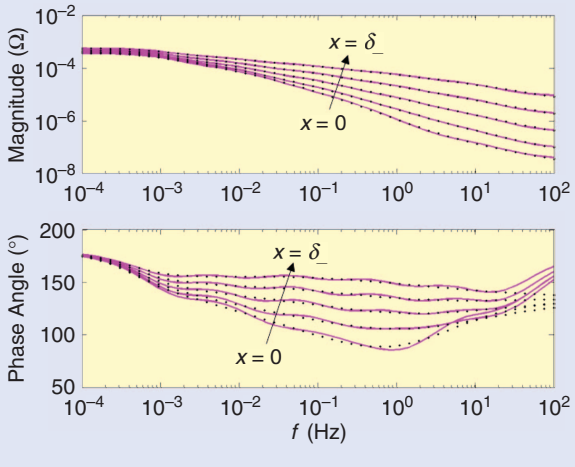

FIGURE 5 Result of the model reduction procedure for a transfer function representing the solid-phase Li concentration impedance at the negative electrode solid/electrolyte interface [5]. The frequency response of the infinite-dimensional transfer function (•) is fit with a fifth-order transfer function (–) from 0 to 10 Hz. The phase-angle error increases above 10 Hz.

is commonly sized with equilibrium conditions in mind with the intention of extending the life of the battery when it is stored at 100% SOC. These limits, however, do not exploit the full capability of the battery. Under high-rate operation, the maximum voltage limit can often be exceeded without damage. For example, it is shown in [15] that pulse charging the 6-Ah cell to the same negative-electrode phase-potential limit ($\phi_{s-e}(\delta_-,t) \geq 80\,\text{mV}$) encountered at equilibrium at 100% SOC increases usable charge power by 22% and usable energy by 212%. These results, which are based on U.S. Department of Energy's Partnership for Next Generation Vehicles test procedures at room temperature, are compared to results when controlled to the manufacturer's 3.9-V limit. For an HEV application, where the battery is sized for power, the cost savings achieved by downsizing this battery would be upwards of $400 per vehicle.

At low temperatures, even more significant performance gains can be achievable with electrochemical control. Figure 6 shows simulation results taken from [10] in which a 6-Ah cell is charged using repeated 10-s pulses interspersed with 10-s periods of rest. The initial condition is 0% SOC and −30 °C. In case A of Figure 6, the charge pulses are controlled to the manufacturer's 3.9-V maximum limit.

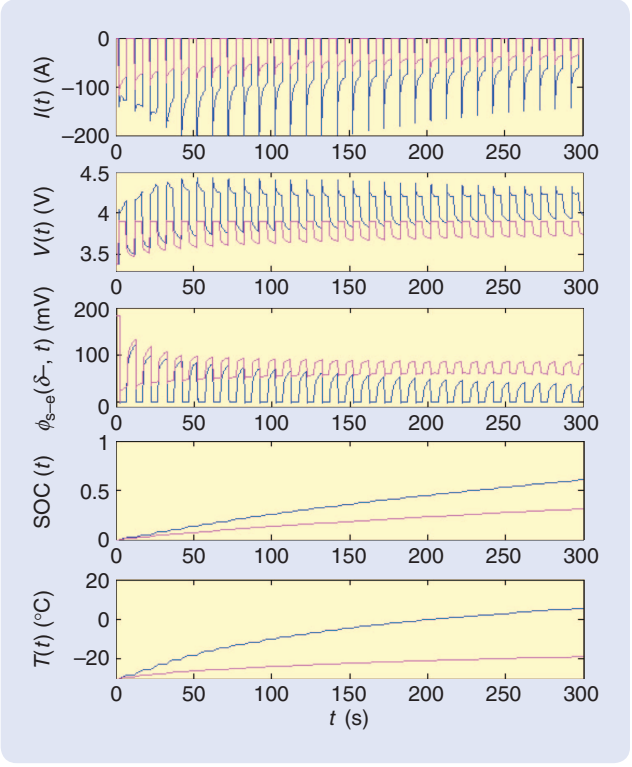

FIGURE 6 Comparison of pulse charging controlled to a fixed maximum voltage limit (purple lines, typical practice) and pulse charging controlled to an internal Li-plating side reaction limit (blue lines, electrochemical control method) [10]. Control to the latter electrochemical limit enhances charge performance at cold temperatures compared to standard practice.

In case B, the charge pulses are controlled to an internal potential limit at which metallic Li begins to plate at the electrode surface ($\phi_{s-e}(\delta_-, t) \geq 0\,\text{V}$), instead of undergoing the nominal charge transfer reaction. For a cell manufacturer, metallic Li plating often limits maximum charge rate at low temperatures.

Comparing the simulation results of Figure 6, control to the internal Li plating limit allows roughly double the charge current rate relative to the fixed external voltage limit. The higher current generates significant internal heating, and brings the electrochemically controlled cell up to nominal operating temperature more quickly. Full recharge is accomplished three times faster compared to the fixed external voltage limit.

In the case of the Li plating-controlled cell, the voltage and current profiles corresponding to the internal limit are highly complex due to temperature-dependent kinetics and transport properties as well as system dynamics. It would be difficult to schedule Li plating limits using an empirical algorithm.

FUTURE DIRECTIONS

While the simulated results are promising, the electrochemical control method described above has not been experimentally validated. Also, it is reasonable to expect that not all of the performance improvement shown in Figure 6 may be achievable due to additional limitations, such as material stress and fracture, which might come into play. Nonetheless, the performance improvement is compelling enough to warrant further research to prove the concept's viability through experiments. A method to rapidly identify the low-order model directly from experimental data, rather than from a full set of electrochemical parameters, is a necessary first step.

Adaptive algorithms are desirable to track health and accommodate performance degradation throughout the battery's life. Adaptive methods may be challenging for the present algorithm, however. The present algorithm, with a reference model identified using the procedure shown in Figure 4, achieves fast computation thanks to a large number of precalculated residue vectors $\mathbf{r}_k$ stored in lookup tables. The method, however, provides no means for adapting these residue vectors to maintain accuracy as the cell ages [6]. Perhaps a few preselected degradation parameters might be tracked by means of lookup tables with added dimensions to map the response to the changing parameters. For a model with four to seven states, the memory requirement may be unduly large. Improved methods to map residue vectors to the physical electrochemical model parameters are therefore needed. A fractional derivative representation [16], for example, may be able to reduce the model down to two or three states and enable adaptation.

Other approaches to electrochemical model formulation and reduction may be preferred in some cases. A

hybrid equivalent circuit/electrochemical model, for example, may be well suited when a single electrode is known to limit performance. In cases where spatial nonuniformities are small, a lumped model [17] could produce a less memory-intensive algorithm that retains a direct connection to its electrochemical model parameters. Furthermore, in cases where distributed nonlinearities are significant, model reduction through partial orthogonal (Karhuenen-Loeve-Galerkin) decomposition methods [18], [19] could provide more accurate prediction, though the iteration required would yield a more computation-intensive algorithm. The model-reduction method shown in Figure 4 approximates distributed nonlinearities with fast, explicit computation and thus provides a compromise between simple lumping and complex partial orthogonal decomposition methods. The reduction procedure may be suitable for control of other distributed systems such as fuel cells and chemical processes.

CONCLUSIONS

While advanced batteries have enabled great improvements in society's mobility and energy efficiency, the high cost of batteries hampers further market penetration. Battery technology improvements are most often sought in electrochemical laboratories. But control engineers have an important role to play in advancing this technology. As a first step, the battery community must begin to merge the knowledge base of control theorists and practitioners with that of electrochemists and materials scientists.

Robust integration of a battery into a high-power system is an experimentally burdensome process, with significant capital resources devoted to cycling batteries under a variety of power profiles and temperatures for several years to ensure reliability. A physics-based approach to battery integration offers the opportunity for streamlining control validation by setting physical limits that are accurate for all possible temperatures and operating scenarios.

By introducing electrochemical state algorithms to existing Li-ion technology, usable power increases in the range of 20–50% seem possible for the entire family of Li-ion chemistries. Performance improvements may also be possible for Ni-MH chemistries with extensions to the method. In the end, improved accuracy and less conservative control limits mean more usable power and energy can be achieved for any given battery system. The outcome is that a smaller battery can provide the same capability, reducing both cost and weight.

AUTHOR INFORMATION

Kandler A. Smith (kandler.smith@nrel.gov) is a senior engineer in Transportation Technologies and Systems at the U.S. Department of Energy's National Renewable Energy Laboratory in Golden, Colorado. He obtained the Ph.D. in mechanical engineering from Pennsylvania State University in 2006. Prior to graduate studies, he spent four years with United Technologies Corporation Pratt & Whitney developing jet engine control systems for a vertical takeoff and landing aircraft. He is a member of the IEEE, the Electrochemical Society, and the Society for Automotive Engineers. His research includes electric-drive vehicle systems, battery electrochemical/thermal characterization and modeling, and battery-life predictive modeling.

REFERENCES

[1] G. L. Plett, "Extended Kalman filtering for battery management systems of LiPB-based HEV battery packs—Part 3. State and parameter estimation," *J. Power Sources*, vol. 134, pp. 277–292, 2004.

[2] M. Verbrugge and B. Koch, "Generalized recursive algorithm for adaptive multiparameter regression," *J. Electrochem. Soc.*, vol. 153, pp. A187–A201, 2006.

[3] T. Fuller, M. Doyle, and J. Newman, "Simulation and optimization of the dual lithium ion insertion cell," *J. Electrochem. Soc.*, vol. 141, pp. 1–10, 1994.

[4] K. A. Smith, C. D. Rahn, and C.-Y. Wang, "Model order reduction of 1D diffusion systems via residue grouping," *ASME J. Dyn. Syst. Meas. Control*, vol. 130, pp. 011012:1–011012:8, 2008.

[5] K. A. Smith, C. D. Rahn, and C.-Y. Wang, "Control oriented 1D electrochemical model of lithium ion battery," *Energy Convers. Manage.*, vol. 48, pp. 2565–2578, 2007.

[6] K. A. Smith, C. D. Rahn, and C.-Y. Wang, "Model-based electrochemical estimation and constraint management for pulse operation of lithium ion batteries," *IEEE Trans. Contr. Syst. Technol.*, to be published.

[7] R. J. Brodd and K. Tagawa, "Lithium-ion cell production process," in *Advances in Lithium-Ion Batteries*, W. A. van Schalkwijk and B. Scrosati, Eds. New York: Plenum, 2002, pp. 267–288.

[8] A. Lasia, "Electrochemical impedance spectroscopy and its applications," in *Modern Aspects of Electrochemistry*, vol. 32, B. E. Conway, J. Bockris, and R. E. White, Eds. Norwell, MA: Kluwer, 1999, pp. 143–248.

[9] I. Ong and J. Newman, "Double-layer capacitance in a dual lithium ion insertion cell," *J. Electrochem. Soc.*, vol. 146, pp. 4360–4365, 1999.

[10] K. A. Smith, "An electrochemical/thermal state algorithm for monitoring of high power lithium-ion batteries," in *Proc. 211th Electrochemical Society Meeting*, Chicago, IL, May 6–10, 2007.

[11] Y. Chen and J. Evans, "Heat transfer phenomena in lithium/polymer-electrolyte batteries for electric vehicle application," *J. Electrochem. Soc.*, vol. 140, pp. 1833–1838, 1993.

[12] J. Christensen and J. Newman, "A mathematical model of stress generation and fracture in lithium manganese oxide," *J. Electrochem. Soc.*, vol. 153, pp. A1019–A1030, 2006.

[13] X. Zhang, W. Shy, and A. M. Sastry, "Numerical simulation of intercalation-induced stress in Li-ion battery electrode particles," *J. Electrochem. Soc.*, vol. 154, pp. A910–A916, 2007.

[14] A. Bemporad, "Reference governor for constrained nonlinear systems," *IEEE Trans. Automat. Contr.*, vol. 43, pp. 415–419, 1998.

[15] K. A. Smith and C.-Y. Wang, "Power and thermal characterization of a lithium-ion battery pack for hybrid-electric vehicles," *J. Power Sources*, vol. 160, pp. 662–673, 2006.

[16] J. Sabatier, M. Aoun, A. Oustaloup, G. Grégoire, F. Ragot, and P. Roy, "Fractional system identification for lead acid battery state of charge estimation," *Signal Process.*, vol. 86, pp. 2645–2657, 2006.

[17] S. Santhanagopalan and R. E. White, "Online estimation of the state of charge of a lithium ion cell," *J. Power Sources*, vol. 161, pp. 1346–1355, 2006.

[18] A. Chatterjee, "An introduction to the proper orthogonal decomposition," *Current Sci.*, vol. 78, pp. 808–817, 2000.

[19] J. A. Atwell and B. B. King, "Reduced order controllers for spatially distributed systems via proper orthogonal decomposition," *SIAM J. Sci. Comput.*, vol. 26, pp. 128–151, 2005.